Neoplasia 61 (2025) 101140

Contents lists available at ScienceDirect

Neoplasia

journal homepage: www.elsevier.com/locate/neo

Original Research

Sialylated IgG-activated integrin β4-Src-Erk axis stabilizes c-Myc in a p300 lysine acetyltransferase-dependent manner to promote colorectal cancer liver metastasis

Jing Chen [a], Shenghua Zhang [b,c,d], Xinmei Huang [b,c,d], Qianqian Wang [b,c,d], Weiyan Xu [b,c,d], Jing Huang [b,c,d], Yuming Su [a], Qinkun Sun [e], Xiaojuan Du [f], Baocai Xing [a,*], Xiaoyan Qiu [b,c,d,**]

[a] Hepatopancreatobiliary Surgery Department I, Key Laboratory of Carcinogenesis and Translational Research (Ministry of Education/Beijing), Peking University Cancer Hospital & Institute, Beijing, 100142, China
[b] Department of Immunology, School of Basic Medical Sciences, Peking University, Beijing, 100191, China
[c] NHC Key Laboratory of Medical Immunology, Peking University, Beijing, 100191, China
[d] Medicine Innovation Center for Fundamental Research on Major Immunology-related Diseases, Peking University, Beijing, 100191, China
[e] Department of Obstetrics and Gynecology, Peking University Third Hospital, Beijing, 100191, China
[f] Department of Cell Biology, School of Basic Medical Sciences, Peking University, Beijing, 100083, China

ARTICLE INFO

Keywords:
Sialylated IgG
Colorectal cancer liver metastasis
c-Myc
p300
Erk

ABSTRACT

Background: Liver metastasis is a leading cause of colorectal cancer mortality. Therefore, the underlying mechanism and potential therapeutic target of colorectal cancer liver metastasis urge to be found. Mounting evidence indicates that cancer-derived sialylated IgG promotes tumor formation and progression. However, the role of sialylated IgG in colorectal cancer liver metastasis remains undefined.

Materials and methods: Analysis of sialylated IgG in paired tumor tissues and adjacent normal tissues from 65 colorectal cancer patients was performed using immunohistochemical staining. Functional assays of sialylated IgG were explored in vitro and in vivo. The downstream target of sialylated IgG was investigated by performing gene-set enrichment analysis, ubiquitination assay, cycloheximide chase assay, acetylation assay and co-immunoprecipitation.

Results: Here, our investigation reveals that sialylated IgG is significantly upregulated in colorectal cancer and that the increase of IgG is positively associated with liver metastasis and poor overall survival in colorectal cancer patients. Sialylated IgG promotes colorectal cancer cell migration, invasion and liver metastasis. Notably, anti-sialylated IgG antibody effectively blocks colorectal cancer liver metastasis in mouse models. Mechanistically, sialylated IgG upregulates c-Myc protein level by decreasing c-Myc ubiquitination. Moreover, we find that p300/CBP can stabilize c-Myc by reducing c-Myc ubiquitination. Overexpression of p300/CBP protects c-Myc protein level from sialylated IgG-knockdown in a lysine acetyltransferase activity-dependent manner. Furthermore, sialylated IgG upregulates p300 protein level through integrin β4-FAK-Src-Erk signaling.

Conclusion: Collectively, these results indicate that a novel sialylated IgG-integrin β4-FAK-Src-Erk-p300-c-Myc signaling pathway promotes colorectal cancer liver metastasis, thus providing potential therapeutic targets for colorectal cancer liver metastasis.

Abbreviations: CRC, colorectal cancer; CRLM, colorectal cancer liver metastasis; EMT, epithelial-to-mesenchymal transition; UPS, ubiquitin-proteasome system; T, threonine; S, serine; KAT, lysine acetyltransferase; SIA-IgG, sialylated IgG; siRNA, small interfering RNA; IF, immunofluorescent; IP, immunoprecipitation; Co-IP, co-immunoprecipitation; IHC, immunohistochemical; COAD, colon adenocarcinoma; READ, rectum adenocarcinoma; TCGA, the cancer genome atlas program; GTEx, the genotype-tissue expression project; GSEA, gene-set enrichment analysis; FACS, fluorescence-activated cell sorting; CHX, cycloheximide; A, alanine; Y, tyrosine; E, glutamic acid.

* Corresponding author at: Hepatopancreatobiliary Surgery Department I, Key Laboratory of Carcinogenesis and Translational Research (Ministry of Education/Beijing), Peking University Cancer Hospital & Institute, Beijing, 100142, China.
** Corresponding author at: Department of Immunology, School of Basic Medical Sciences, Peking University, Beijing, 100191, China.
E-mail addresses: xingbaocai88@sina.com (B. Xing), qiuxy@bjmu.edu.cn (X. Qiu).

https://doi.org/10.1016/j.neo.2025.101140
Received 14 November 2024; Received in revised form 10 February 2025; Accepted 12 February 2025

Introduction

Colorectal cancer (CRC) is the second leading cause of cancer mortality worldwide [1]. Metastasis is the major cause of death of CRC patients. Liver is the most frequent site of metastasis for CRC, owing to the venous blood from the gastrointestinal system returning to the portal vein circulation [2]. Therefore, elucidating the mechanism of colorectal cancer liver metastasis (CRLM) and identification of therapeutic targets to improve the prognosis of patients with CRC are necessary.

The *MYC* oncogene (also known as c-Myc) encodes the transcription factor c-Myc protein, with two paralogues, namely *MYCL* and *MYCN*, belonging to a superfamily. As one of the most commonly activated genes in human cancers, c-Myc is a master regulator of hallmarks of cancer, contributing to cancer invasion and metastasis [3]. High c-Myc expression promotes CRLM by a variety of different mechanisms, including inducing epithelial-to-mesenchymal transition (EMT) [4], promoting tumor immune evasion [5] and enhancing tumor chemotherapeutic resistance [6]. c-Myc expression is highly regulated by both transcriptional and post-translational mechanisms. Several post-translational modifications, including phosphorylation, acetylation and ubiquitination, have been implicated in the regulation of c-Myc protein stability. The most prominent route for c-Myc protein targeted degradation is the ubiquitin-proteasome system (UPS). A number of ubiquitin ligases, such as TRIM32 [7] and UBE3B [8], and deubiquitinases, such as OTUB1 [9], USP37 [10] and USP10 [11], have been identified to regulate c-Myc protein stability. c-Myc destabilization and degradation are commonly affected by two conserved phosphorylation sites: threonine (T) 58 [12] and serine (S) 62 [13]. c-Myc is also an acetylation target of several lysine acetyltransferases (KATs), including p300, CBP [14,15], GCN5, PCAF and Tip60 [16,17], and c-Myc acetylation facilitates its stabilization [18,19]. c-Myc has been widely considered to be "undruggable" and direct targeting of c-Myc is very challenging [20]. Thus, various molecular mechanisms that regulate c-Myc protein stability are promising therapeutic targets.

The KATs p300 and CBP are often referred to as p300/CBP due to their sequence homology, functional overlap and co-operation. p300/CBP have recently been identified as critical tumorigenic drivers, functioning in CRC metastasis and proliferation through diverse mechanisms, including acetylating histones and serving as a bridge to connect transcription factors to chromatin and the basal transcriptional machinery [21–23]. The regulation of p300 has been investigated previously. Changes of phosphorylation as well as auto-acetylation of p300 have been shown to associate with its degradation, which depends on proteasome or lysosome [21,24,25]. The relationship between p300/CBP and c-Myc in CRC remains to be identified.

Immunoglobulins are generally produced by B cells and defend us against infection. However, more evidence has shown that immunoglobulins are also expressed in non-B cells, including neurons [26], hepatocytes [27], spermatogenic cells [28] and cardiomyocytes [29]. Of note, epithelial cancers, including breast cancer [30], lung cancer [31,32], prostate cancer [33] and pancreatic ductal adenocarcinoma [34], and cancer cell lines [35] have high IgG expression levels. This IgG is named as cancer-derived IgG. The basic structure of IgG consists of two identical light (L) chains and two identical heavy (H) chains, which are divided into the variable and constant (C) regions. The heavy chains contain three constant regions (C_H1, C_H2 and C_H3). As a common glycoprotein, IgG is frequently glycosylated at a classic asparagine (Asn) 297 site, located in C_H2 domain [36]. Our study reveals that cancer-derived IgG possesses unique N-glycosylation and a high level of sialic acid modification at the Asn162 site of the C_H1 domain [32], which is known as sialylated IgG (SIA-IgG). Glycosylated cancer-derived IgG relying on its unique sialylation modification at the Asn162 site plays an important role in cancer migration [32], stemness maintenance [31] and immune evasion [37]. Furthermore, the high level of sialylation modification at Asn162 site of SIA-IgG is specifically recognized by RP215 antibody [32]. Although it was previously reported that the expression of SIA-IgG was upregulated and associated with poor overall survival in CRC patients [38], the function and the underlying molecular mechanism of SIA-IgG in CRLM remain unclear. Thus, elucidating the role and functional mechanism of SIA-IgG and its potential as a therapeutic target in CRLM is essential.

In the present study, we show that high SIA-IgG expression drives colorectal cancer to spread to liver both in vitro and in vivo by reducing c-Myc ubiquitination and degradation and stabilizing c-Myc. In addition, we characterize that SIA-IgG promotes p300/CBP protein levels, which increase c-Myc stability in an acetylation-dependent manner. Moreover, we propose that SIA-IgG interacts with integrin β4 and activates FAK-Src-Erk signaling, leading to the increase of p300 and c-Myc protein levels. Therefore, we evaluate SIA-IgG as an attractive theoretical target for treatment of CRLM.

Materials and methods

Cell culture and reagents

The HT-29, SW480, HCT116 $p53^{-/-}$, HCT116 $p53^{+/+}$ and HCT8 cell lines were from Peking University Center of Human Disease Genomics. LoVo and 293FT cell lines were obtained from the Cell Resource Center (Beijing, China). SW620 cell line was obtained from the American Type Culture Collection (Manassas, VA, USA). Cells were maintained in RMPI 1640 or Dulbecco's modified Eagle's medium respectively, supplemented with 10 % fetal bovine serum and 1 % penicillin-streptomycin solution. All cell lines were cultured in a 5 % CO_2 at 37 °C humidified atmosphere.

Cell transfection or infection

Cells were transfected with plasmids or small interfering RNA (siRNA) according to the polyethylenimine (Serochem) or lipofectamine3000 (Sigma) reagent protocol. Plasmids and siRNA were supplied by MailGene (Beijing, China) and RiboBio (Guangzhou, China) respectively. Transfer plasmid, psPAX2 plasmid and pVSVG plasmid at a ratio of 2:1:1 was packaged by 293FT cells. After 60 h, the cell supernatant was harvested and concentrated using PEG 8000, preserved at −80°C. Cells were infected by lentivirus concentration solution using polybrene.

Plasmids construction

c-Myc sequence was cloned into pcDNA3.1 vector with flag tagged. Fast Site-Directed Mutagenesis Kit (TIANGEN) was used for single or double mutant plasmids construction.

Western blotting

Cell pellet was lysed in RIPA lysis (LEAGENE) with protease inhibitor cocktail (Roche) and phosphatase inhibitor PhosSTOP (Roche) and reduced and denatured with 5 × loading buffer and DTT at 99 °C for 15 min. And western blotting was performed to analyze protein according to the standard protocol. Information on the antibodies is listed in Table S1.

Transwell migration and invasion assays

Cells were seeded in serum-free medium on the uncoated or Matrigel (Corning)-coated upper layer of the transwell chamber with 8 μm pores (FALCON), and 750 μL medium containing 10 % fetal bovine serum was placed below the cell permeable membrane. After 36 h, the cells migrating through the membrane were stained with 1 % crystal violet solution containing paraformaldehyde and counted using ImageJ software.

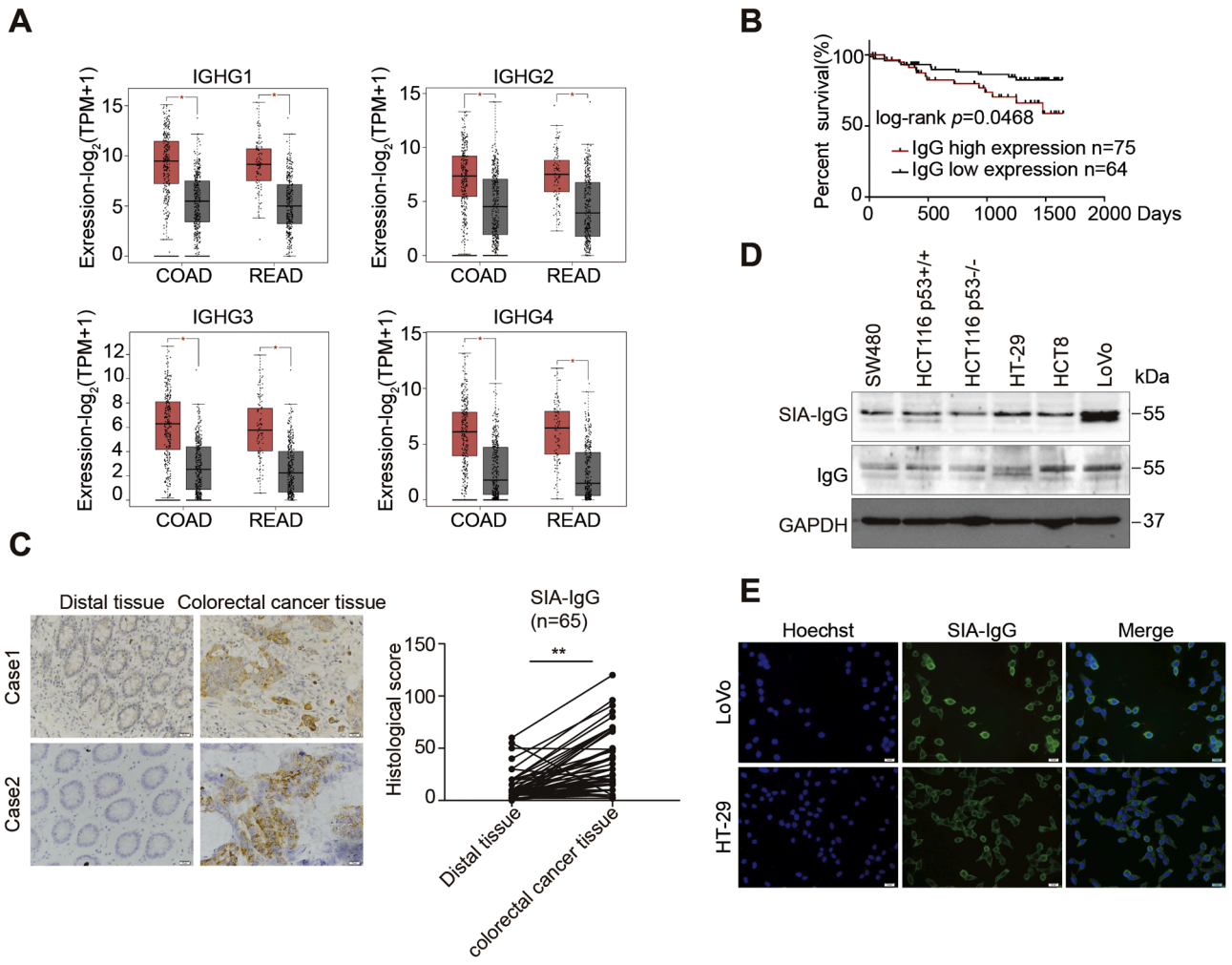

Fig. 1. Upregulation of SIA-IgG is correlated with poor outcome of colorectal cancer patients. (A) The expression of IGHG1, IGHG2, IGHG3 and IGHG4 in COAD (n = 275) and RAED (n = 92), normal colon (n = 349) and rectal (n = 318) tissues in the TCGA and GTEx databases (red column represents tumor tissues, grey column represents normal tissues). (B) Overall survival of patients with CRC stratified by IgG protein level based on a proteomic dataset (n = 139) using the Kaplan–Meier method. (C) Representative IHC staining of SIA-IgG in matched colorectal cancer and non-cancerous tissues (left panel) (n = 65). Summary of SIA-IgG expression in matched colorectal cancer and non-cancerous tissue (right panel). **, $p < 0.01$. Scale bars, 20 μm. (D) Western blot analysis of SIA-IgG and IgG protein levels in CRC cell lines. (E) The expression and localization of SIA-IgG in LoVo and HT-29 cells were analyzed by IF using anti-SIA-IgG antibody (green) and Hoechst (blue). Scale bars, 20 μm.

RNA isolation and Real-time quantitative PCR

Total RNA was isolated from cell samples according to TRIzol (Sigma) Reagent protocol. Then, 2 μg total RNA was reverse-transcribed into cDNA using reverted first strand cDNA synthesis kit (Thermo Fisher Scientific). The cDNA was diluted at a ratio of 1:50. qPCR was performed using Hieff qPCR SYBR Green Master Mix (Yeasen). The expression level of mRNA relative to GAPDH was calculated by the $2^{-\Delta\Delta CT}$ method. The qPCR primers are shown in Table S2.

Immunofluorescent (IF) staining

Cells seeded on cover glasses were washed 3 times with PBS, then fixed with acetone for 5 min at room temperature. After being blocked with 10 % goat sera for 30 min at room temperature, cells were incubated with primary antibody overnight at 4 °C. Then cells were incubated with FITC-conjugated anti-mouse secondary antibody at 1:200 in PBS for 1 h at room temperature in dark. Cells were incubated with Hoechst at 1:200 for 5 mins at room temperature, then mounted with a drop of 50 % glycerol.

Immunoprecipitation (IP) and Co-immunoprecipitation (Co-IP)

Cells were harvested and lysed in lysis buffer (150 mM NaCl, 50 mM Tris-HCl pH 7.4, 1 % NP-40, 10 % glycerol) with protease inhibitor cocktail (Roche). Cell supernatants were incubated with anti-Flag magnetic beads (Abmart) on a roller shaker overnight at 4°C. After being washed with washing buffer (150 mM NaCl, 50 mM Tris-HCl pH 7.4, 0.1 % NP-40) for five times, the bound flag fusion protein was eluted with SDS-PAGE sample buffer, then boiled, and analyzed by western blotting. For detection of c-Myc acetylation, cells before being harvested were treated with trichostatin A (Solarbio) and nicotinamide (Sigma) for 6 h, and trichostatin A and nicotinamide were also added into the lysis buffer.

Animal studies

For the construction of nude mouse models of colorectal cancer liver metastasis, LoVo cells infected with negative control or shIgG lentivirus concentration solution were prepared for mouse models. After male nude mice were anesthetized with tribromoethanol (intraperitoneal injection, 100 μL (volume) /10 g (weight), biopike). A 1 cm left subcostal

Table 1.
Correlation between IgG protein level in CRC patients and their clinicopathological features.

Clinicopathological features	Number	IgG low expression n (%)	IgG high expression n (%)	*p* value
Gender				
Male	97	51(68.0)	46(66.7)	$p = 1.000$
Female	47	24(32.0)	23(33.3)	
Age (years)				
< 65	71	27(36.0)	44(63.8)	$p = 0.001$**
≥ 65	73	48(64.0)	25(36.2)	
Liver metastasis				
No	74	45(69.2)	29(42.0)	$p = 0.002$**
Yes	60	20(30.8)	40(58.0)	
CEA				
< 5 ng/mL	73	37(48.7)	36(55.4)	$p = 0.500$
≥ 5 ng/mL	68	39(51.3)	29(44.6)	
CA19-9				
< 37 U/mL	104	61(81.3)	43(66.2)	$p = 0.053$
≥ 37 U/mL	36	14(18.7)	22(33.8)	

Data for IgG expression is missing for two.
Data for CEA, CA19-9 were missing for three and four patients respectively.
** $p < 0.01$.

incision was made, exposing and pulling out the spleen. 2.0×10^6 cells in 75 uL PBS were gently and slowly injected into the spleen, then close the peritoneum and skin with stitches. For therapy of colorectal cancer liver metastasis in nude mice, RP215 antibody or mIgG (5 mg/kg) were injected via tail veins twice a week. At indicated days, the mice were euthanized, liver samples were harvested.

For the xenograft tumor models, colon cancer cells SW480 (5×10^6 cells in 150 μL of PBS containing 50 μL of Matrigel) (Corning, New York, USA) were injected subcutaneously into the axilla of the NOD-SCID mice. Tumor growth was monitored and the tumor volume was calculated as (width^2 × length)/2. And RP215 or mIgG was injected with 5 mg/kg respectively every three days via intraperitoneal administration.

All animal experiments were approved by Institutional Animal Care and Use Committee of Peking university (permit number: PUIRB-LA2022691).

Immunohistochemical (IHC) staining

Colon cancer tissue and distal tissue were obtained from Peking University Peoples' Hospital. And collection of these samples was approved by the Clinical Research Ethics Committee of Peking University Peoples' Hospital (permit number: 2015PHB212-01). Also, informed consents were obtained from participating patients. Formalin-fixed tissue sections were placed in xylene for deparaffinization and in graded ethanol for rehydration. Antigen retrieval was performed using Tris/EDTA-2Na buffer (pH 9.0). 3 % H_2O_2 was incubated with slides at room temperature for 10 min to suppress endogenous peroxidase. The sections were blocked with goat sera and incubated with primary antibody overnight at 4 °C. The slides were rinsed 3 × 5 min in PBS, then incubated with anti-mouse/rabbit IgG horseradish peroxidase (Dako) at room temperature for 20 min. and detected using diaminobenzidine. The score was given by the multiply of the staining intensity (no staining, 0; weak staining, 1; moderate staining, 2; strong staining, 3) and the percentage (0-100 %) of positive area.

Statistical analysis

The log-rank test was used to analyze Kaplan-Meier survival curve. Fisher's exact test was used to analyze the relationship between the expression of IgG protein and clinicopathological features. Gene set enrichment pathway was performed by GSEA software. The significance of the differences was analyzed by two-tailed Student's *t*-test. Significant differences were indicated by $p < 0.05$. The statistical analyses were performed using SPSS 27.0.

Results

SIA-IgG is upregulated in CRC and positively correlated with poor outcome and liver metastasis

To explore the expression of IgG in CRC, we first analyzed IgG mRNA expression level in colon adenocarcinoma (COAD, $n = 275$), rectum adenocarcinoma (READ, $n = 92$) and normal colon ($n = 349$) and rectal ($n = 318$) tissues from the cancer genome atlas program (TCGA) and the genotype-tissue expression project (GTEx) [39], and found that IgG was substantially elevated in COAD and READ compared with the normal tissues (Fig. 1A). We also analyzed the publicly accessible CRC proteomic dataset [40], and found the abundance of IgG in CRC samples ($n = 139$). Survival analysis revealed that IgG high expression predicted shorter overall survival compared to IgG low expression group (Fig. 1B). To further identify the clinical relevance of IgG in CRC [40], we analyzed the relationship between IgG protein expression level and clinical features, and found that the expression level of IgG was positively associated with CRLM (Table 1). Furthermore, we performed IHC staining using RP215 antibody to evaluate SIA-IgG expression in 65 matched tissue specimens, including the surgical margin (as the non-cancerous tissues) and CRC tissues. The result showed that SIA-IgG was expressed at higher levels in cancer cells compared to normal epithelial cells. Moreover, SIA-IgG in colon cancer only highly expressed in a small number of cancer cells, such as the high invasive potential at the leading edge of the tumor front (Fig. 1C). Various levels of SIA-IgG and IgG expression could be detected in CRC cell lines, with higher SIA-IgG expression level in the high metastatic cell line LoVo (Fig. 1D). The IF assays also showed that SIA-IgG expressed in LoVo and HT-29 cells (Fig. 1E). In summary, these data reveal that SIA-IgG is upregulated in CRC, and positively associated with liver metastasis and poor prognosis.

SIA-IgG promotes CRC cells migration, invasion and liver metastasis

To explore the potential role of SIA-IgG on CRLM, SIA-IgG in LoVo and HT-29 cells was knocked down, and we observed that knockdown of SIA-IgG resulted in a decrease of migration and invasion of LoVo and HT-29 cells (Fig. 2A). To characterize the significance of the sialylation modification at the Asn162 site of SIA-IgG, we first blocked SIA-IgG with anti-SIA-IgG antibody RP215 (Supplementary Fig. 1A) and RP215 antibody treatment drastically inhibited migration and invasion of LoVo and HT-29 cells (Fig. 2B). Moreover, SIA-IgG protein was purified from ovarian carcinoma ascites by RP215-affinity chromatography and evaluated by western blotting (Supplementary Fig. 1B), then SIA-IgG, non-SIA-IgG (the control-IgG of flow-through) or a vehicle control (PBS) was used to treat LoVo and HT-29 cells. The result showed that SIA-IgG can substantially promote CRC cells migration and invasion (Fig. 2C).

To further investigate whether SIA-IgG promotes metastasis of CRC in vivo, we established liver metastasis mouse models of colorectal cancer by intrasplenic implantation with LoVo cells, which were transfected with shIgG or shNC lentivirus supernatant, and confirmed that SIA-IgG was significantly suppressed (Fig. 2D). The results showed that the numbers of metastatic tumors and maximum tumor sizes were significantly reduced in shIgG group compared with the control group (Fig. 2E-H). We also constructed intrasplenic injection models of colorectal cancer metastasis to the liver in nude mice, followed by tail vein injection with RP215 (5 mg/kg) or mIgG (as a negative control) twice a week. RP215 treatment significantly decreased liver metastatic tumor numbers. The maximum tumor sizes between RP215 group and mIgG

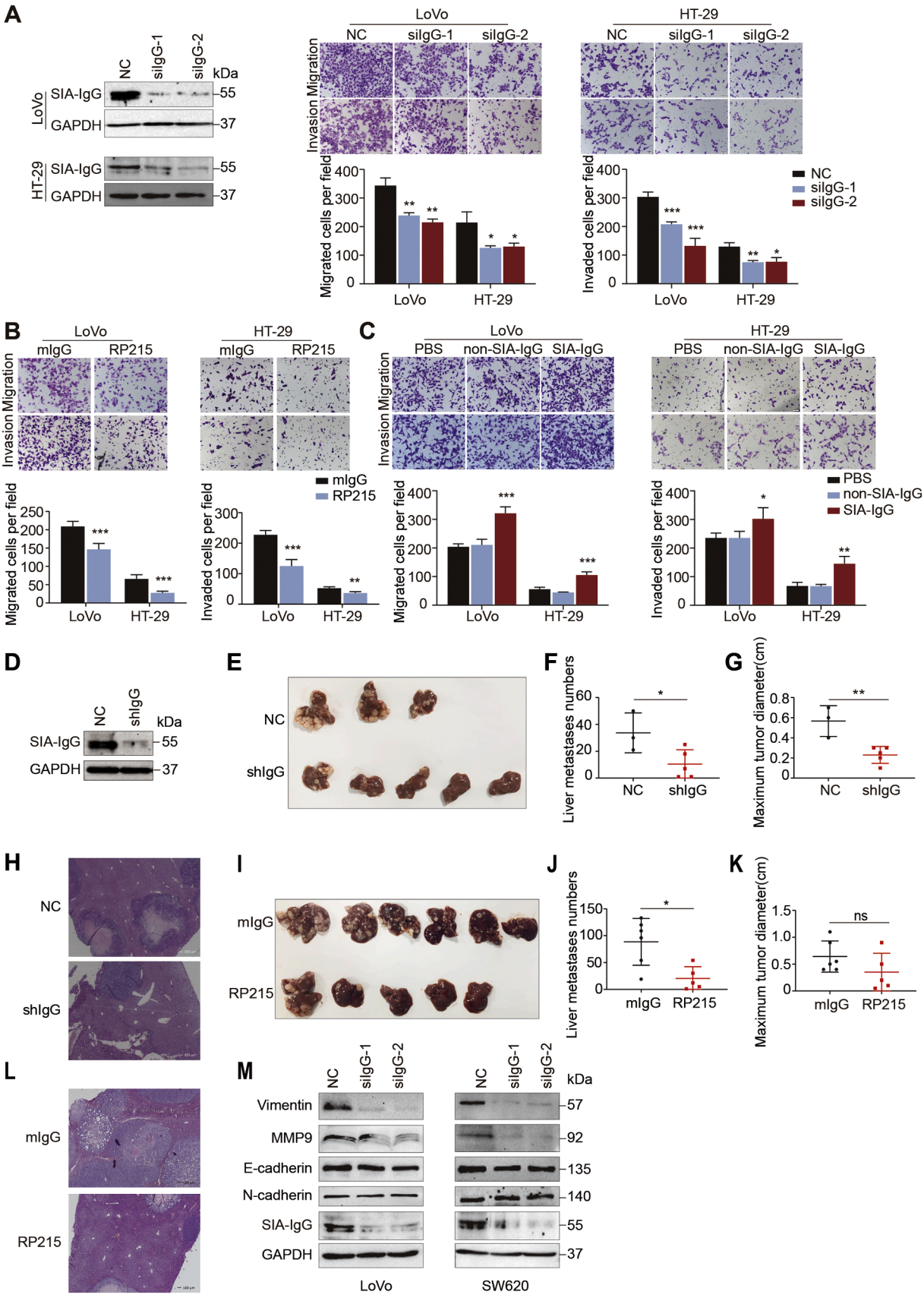

(caption on next page)

Fig. 2. SIA-IgG increases CRC cells migration, invasion and liver metastasis. (A) SIA-IgG expression levels were determined by western blotting in SIA-IgG knockdown CRC cells. The effect of SIA-IgG knockdown on CRC cells migration and invasion was assessed by transwell assays. The data are presented as the mean ± SD (*, $p < 0.05$, **, $p < 0.01$, ***, $p < 0.001$). Differences between groups were evaluated with a two-tailed paired Student's *t*-test. Scale bars, 50 μm. (B) Migration assays and invasion assays were performed using LoVo and HT-29 cells treated with 50 μg/mL RP215 or mIgG. Representative results and quantification are shown. The data are presented as the mean ± SD. (**, $p < 0.01$, ***, $p < 0.001$). Differences between groups were evaluated with a two-tailed paired Student's *t*-test. Scale bars, 50 μm. (C) Migration assays and invasion assays were conducted using LoVo and HT-29 cells treated with PBS, non-SIA-IgG (30 μg/mL) or SIA-IgG (30 μg/mL). Representative results and quantification are shown. The data are presented as the mean ± SD. (**, $p < 0.01$, ***, $p < 0.001$). Differences between groups were evaluated with a two-tailed paired Student's *t*-test. Scale bars, 50 μm. (D) LoVo cells were stably transfected with shIgG or shNC lentivirus, and SIA-IgG expression was assessed by western blot before cells were injected into spleen. (E) Representative macroscopic images of the liver metastases upon intrasplenic injection of NC (upper panel) and shIgG (lower panel) LoVo cells in nude mice. (F) Numbers of metastatic tumors of NC group ($n = 3$) and shIgG group ($n = 5$) LoVo cells in nude mouse models of colorectal cancer liver metastasis. The data are presented as the mean ± SD. (*, $p < 0.05$). Differences between groups were evaluated with a two-tailed unpaired Student's *t*-test. (G) Maximum diameters of liver metastases of LoVo NC ($n = 3$) and shIgG ($n = 5$) cells in nude mouse models of colorectal cancer liver metastasis were measured. The data are presented as the mean ± SD. (*, $p < 0.05$). Differences between groups were evaluated with a two-tailed unpaired Student's *t*-test. (H) Representative pictures of hematoxylin and eosin (HE) staining of liver tissue sections from indicated mice. Scale bars, 100 μm. (I) Representative macroscopic images of the liver metastases in nude mice upon intrasplenic injection of LoVo cells treated with RP215 ($n = 5$) or mIgG ($n = 6$) twice a week. (J) Numbers of metastatic tumors of LoVo cells treated with RP215 ($n = 5$) or mIgG ($n = 6$) in nude mouse models of colorectal cancer liver metastasis. The data are presented as the mean ± SD. (*, $p < 0.05$). Differences between groups were evaluated with a two-tailed unpaired Student's *t*-test. (K) Maximum diameters of liver metastases of LoVo cells treated with RP215 ($n = 6$) or mIgG ($n = 5$) in nude mouse models of colorectal cancer liver metastasis were measured. The data are presented as the mean ± SD. (ns, not significant). Differences between groups were evaluated with a two-tailed unpaired Student's *t*-test. (L) Representative pictures of HE staining of liver tissue sections from indicated mice. Scale bars, 100 μm. (M) Western blot analyses of metastasis-related proteins with or without SIA-IgG knockdown in LoVo and SW620 cells.

group tended to decline, though this was not statistically significant (Fig. 2I-L). In addition, no significant fluctuations of body weight were observed in the RP215 group (Supplementary Fig. 2A), suggesting the safety application of RP215 antibody in vivo. EMT has been reported to be implicated in CRLM by enhancing cancer cells mobility and invasion [41–43]. To demonstrate whether EMT is involved in SIA-IgG promoting CRLM, EMT-related molecules were detected in SIA-IgG-silenced cells. Western blot results indicated that Vimentin and MMP9 protein levels were considerably lowered in the SIA-IgG-knockdown group of high metastatic cell lines LoVo and SW620, and E-cadherin and N-cadherin protein levels showed no changes (Fig. 2M). The above results indicate that SIA-IgG encourages metastasis of CRC by promoting EMT.

Given that tumor proliferation and metastatic potential are mutually supportive processes, we aimed to investigate whether SIA-IgG promotes tumor growth. SW480 cells were subcutaneously injected into the NOD/SCID mice. Following treatment with RP215, we observed that RP215 treatment suppressed tumor growth compared to the control group (Supplementary Fig. 3A-D). This finding is consistent with our previous result that knockdown of SIA-IgG inhibits tumor growth in xenograft models [38].

Taken together, these results provide strong evidence that SIA-IgG promotes CRC cells proliferation, migration, invasion and liver metastasis.

SIA-IgG upregulates c-Myc protein level by enhancing c-Myc protein stability

To identify the gene expression changes and signaling pathways involved in SIA-IgG promoting CRLM, we first conducted gene-set enrichment analysis (GSEA) of all quantified proteins based on proteomic profiling of IgG in CRC tissues ($n = 144$) (Fig. 3A), and it revealed MYC_TARGETS_V1 and MYC_TARGETS_V2 signatures as the most strongly downregulated hallmark gene signatures in IgG^{low} CRC samples (Fig. 3B). Next, we determined whether SIA-IgG expression was correlated with c-Myc. SIA-IgG^{high} and SIA-IgG^{low} of LoVo cells were sorted by fluorescence-activated cell sorting (FACS). Immunoblotting using sorted cells revealed that SIA-IgG^{high} cells displayed significantly higher c-Myc level (Fig. 3C). Subsequently, the c-Myc mRNA level was quantified in SIA-IgG^{high} and SIA-IgG^{low} of LoVo cells using RT-PCR. The result showed no significant reduction in c-Myc mRNA level in SIA-IgG^{low} cells compared to that in SIA-IgG^{high} cells (Supplementary Fig. 4A). To examine whether c-Myc can be upregulated by SIA-IgG, LoVo and HT-29 cells were treated with SIA-IgG and non-SIA-IgG (as control). The result showed that c-Myc was upregulated when cells were exogenously added with SIA-IgG purified by RP215-affinity chromatography, but not the control-IgG (Fig. 3D). On the contrary, upon RP215 treatment, c-Myc was significantly downregulated in LoVo and HT-29 cells (Fig. 3E). Together, these results illustrate that SIA-IgG dependent on its sialylation modification at Asn162 site upregulates c-Myc and that c-Myc plays an essential role in SIA-IgG promoting CRLM.

To explore the underlying mechanism of SIA-IgG regulating c-Myc, we first detected c-Myc mRNA and protein levels by RT-PCR and western blot upon silencing SIA-IgG in LoVo and HT-29 cells. We observed no significant reduction of c-Myc mRNA level between SIA-IgG-knockdown and negative control CRC cell lines. However, the c-Myc protein level was significantly decreased in SIA-IgG-depleted cells (Fig. 3F). c-Myc protein level is usually tightly regulated by UPS-mediated protein degradation. Therefore, MG132, which effectively blocks the proteolytic activity of the 26S proteasome complex, was used to determine if SIA-IgG regulated c-Myc relying on UPS. We found that the proteasome inhibitor MG132 blocked SIA-IgG suppression-induced decrease of c-Myc protein (Fig. 3G). The above results suggested that SIA-IgG might regulate c-Myc through ubiquitination-proteasomal degradation. To further confirm this, Flag-c-Myc was overexpressed in LoVo and HT-29 cells with or without silencing SIA-IgG, then the immunoprecipitation assay was done by employing anti-Flag magnetic beads. Indeed, knockdown SIA-IgG increased the ubiquitination level of c-Myc in LoVo and HT-29 cells (Fig. 3H). Consistent with SIA-IgG promotion of c-Myc protein stability, we found that the half-life of c-Myc was shortened by knockdown SIA-IgG in both LoVo and HT-29 cells in cycloheximide (CHX) chase assays (Fig. 3I). Collectively, our data demonstrate that knockdown of SIA-IgG induces ubiquitin-mediated degradation of c-Myc.

Upregulation of c-Myc by SIA-IgG is mediated by p300/CBP KAT activities

Early studies show that c-Myc protein stability is regulated by several mechanisms, prominent among which is phosphorylation at two conserved residues, T58 and S62 [19]. Phosphorylation of c-Myc at S62 contributes to its stabilization [13], whereas phosphorylation of c-Myc at T58 results in its degradation [12]. To determine if SIA-IgG affects T58 and S62 phosphorylation levels of c-Myc, the phosphorylation levels at T58 and S62 and total protein level of c-Myc in SIA-IgG-knockdown LoVo and HT-29 cells were first detected. We found that there was no significant difference between the phosphorylation levels at T58/S62 sites and c-Myc total protein level (Fig. 4A). Moreover, we constructed a panel of c-Myc phospho-deficient mutants, in which alanine (A) substitutes for threonine and serine residues, and phosphomimetic mutants, in which glutamic acid (E) substitutes for threonine and serine residues. In total, the panel contained T58A, S62A, T58/S62A, T58E, S62E and

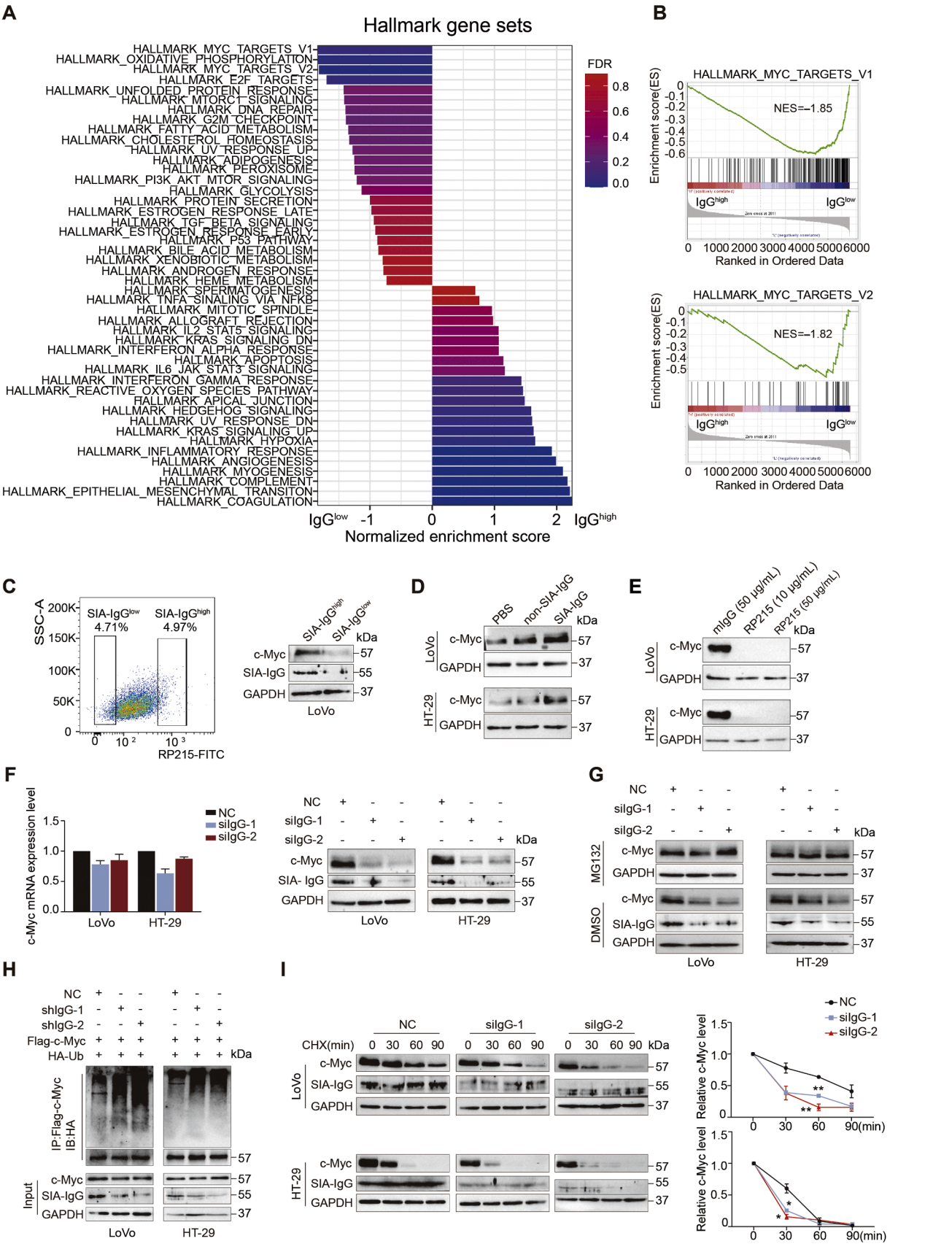

(caption on next page)

Fig. 3. SIA-IgG upregulates c-Myc protein level by enhancing c-Myc protein stability. (A) Hallmark gene sets significantly enriched in CRC samples stratified based on low/high IgG expression from a public proteomic dataset ($n = 144$). (B) GSEA plots of MYC signatures of CRC samples stratified based on low/high IgG expression from a public proteomic dataset ($n = 144$). (C) FACS image of SIA-IgG^{high} and SIA-IgG^{low} cells sorted from LoVo cells. Western blotting analysis of the indicated proteins from SIA-IgG^{high} and SIA-IgG^{low} cells sorted from LoVo cells. (D) Cell lysates from LoVo and HT-29 treated with purified SIA-IgG (30 μg/mL), non-SIA-IgG (30 μg/mL) or PBS were subjected to western blot using the indicated antibodies. (E) Western blotting analysis of the indicated proteins from LoVo and HT-29 cells treated with RP215 or mIgG. (F) Total RNA extracted from SIA-IgG knockdown cells or control cells was reverse-transcribed and subjected to RT-PCR using the c-Myc primers. Western blot analysis of c-Myc protein level from SIA-IgG knockdown cells or negative control cells. (G) c-Myc protein level in LoVo and HT-29 cell with SIA-IgG knockdown in the absence or presence of proteasome inhibitor MG132 (10 μM, 10 h) determined by western blot. (H) LoVo and HT-29 cells were transfected with indicated plasmids and treated with MG132 for 10 h and cell lysates were subjected to immunoprecipitation using anti-Flag magnetic beads. c-Myc ubiquitination was analyzed by western blot. (I) LoVo and HT-29 cells were transfected as indicated and treated with CHX (200 μg/mL) as indicated time points. SIA-IgG and c-Myc protein levels were evaluated by western blotting. Quantification of c-Myc protein levels was summarized (right panel).

T58/S62E mutants. The c-Myc mutant protein levels were evaluated in SIA-IgG-depleted LoVo and HT-29 cells. Neither phospho-deficient c-Myc mutants nor phosphomimetic c-Myc mutants were resistant to loss of SIA-IgG (Fig. 4B and Supplementary Fig. 5A). The above findings indicate that c-Myc is probably not regulated by SIA-IgG through the T58/S62-mediated degradation.

Several lysine acetyltransferases, such as CBP [15], p300 [14], GCN5 [16,17] and Tip60 [44,45], have been previously reported to substantially increase the half-life of c-Myc. To map the acetylation modification on c-Myc protein stability, SIA-IgG was knocked down in LoVo cells followed by Flag-c-Myc overexpression, and we immunoprecipitated Flag-c-Myc and found that the acetylation level of c-Myc strongly decreased after knockdown of SIA-IgG (Fig. 4C). We wonder which KAT is involved in c-Myc regulation from SIA-IgG. First, we transfected a panel of acetyltransferase plasmids, including HA-CBP, HA-p300, HA-Tip60, HA-MOF and HA-PCAF, in LoVo and HT-29 cells respectively. The results showed that both CBP and p300 increased c-Myc protein level (Fig. 4D). To verify that p300/CBP have an effect on the stabilization of c-Myc, we co-expressed HA-p300/HA-CBP in LoVo and HT-29 cells and found that HA-p300 and HA-CBP can increase the half-life of c-Myc (Fig. 4E). Furthermore, we co-expressed HA-p300 or HA-CBP with Flag-c-Myc and conducted IP assays with anti-Flag magnetic beads to detect the c-Myc ubiquitination level in LoVo and HT-29 cells. As shown in Fig. 4F, the c-Myc ubiquitination level decreased by the expression of HA-p300 and HA-CBP. These data suggest that p300/CBP promote c-Myc protein stability.

To confirm whether p300/CBP are the critical factors for SIA-IgG stabilizing c-Myc, we performed a series of rescue assays. HA-p300/HA-CBP and Flag-c-Myc plasmids were transfected into LoVo and HT-29 cells following knockdown SIA-IgG. Immunoblot assays demonstrated that overexpression of p300/CBP could effectively prevent c-Myc downregulation from SIA-IgG knockdown (Fig. 4G). Then, HA-p300/HA-CBP and Flag-c-Myc were reintroduced into the SIA-IgG-silenced LoVo cells, and c-Myc ubiquitination level was evaluated. As shown in Fig. 4H, HA-p300 and HA-CBP can dramatically deceased the c-Myc ubiquitination level in SIA-IgG-depleted cells. Thus, these results indicate that p300/CBP mediate SIA-IgG-induced c-Myc protein stability.

We further examined whether p300/CBP affect c-Myc protein stability through their KAT activities, as previous studies showed that p300/CBP could acetylate c-Myc [15,46]. We overexpressed HA-p300/HA-CBP and Flag-c-Myc in LoVo and HT-29 cells following SIA-IgG knockdown, and cells were exposed to a selective catalytic p300/CBP inhibitor A-485 [47]. As shown in Fig. 4I, A-485 treatment resulted in the marked reduction of c-Myc protein level promoted by p300 and CBP under loss of SIA-IgG condition. Importantly, as LoVo and HT-29 cells were treated with A-485 after SIA-IgG knockdown, the c-Myc protein level reduction induced by SIA-IgG knockdown was diminished (Fig. 4J). These data highlight that the KAT activities of p300/CBP are required for c-Myc protein stabilized by SIA-IgG.

Erk phosphorylation activation is required for SIA-IgG-promoted p300 and c-Myc protein levels

We next addressed the regulation of SIA-IgG on p300/CBP. Upon SIA-IgG suppression in LoVo and HT-29 cells, we observed that p300/CBP protein levels significantly decreased, whereas p300/CBP mRNA expression levels were not notably affected (Fig. 5A). Given that Erk activation increases p300 protein level and KAT activity by directly phosphorylating p300 [48,49] and oncogenic integrin-FAK-Src signalings are related to tumor progress [32], we next whether SIA-IgG regulates p300 through integrin β4-FAK-Src-Erk singalling. Based on our previous work [32], we examined the interaction between SIA-IgG and integrin β4 in LoVo cells. Total lysates of LoVo cells were subjected to co-immunoprecipitation using RP215, followed by western blot to identify integrin β4. The interaction of SIA-IgG and integrin β4 was validated (Fig. 5B). Then, we analyzed the activation of FAK and Src in LoVo and HT-29 cells after knockdown of SIA-IgG, and found that the phosphorylation levels of FAK at tyrosine (Y) 397 and Y925 and Src at Y416 were reduced in SIA-IgG-deficiency cells (Fig. 5C). Accordingly, Src possesses a regulatory activity on Erk1/2 and Src facilitates activation of Erk1/2 [50,51]. In this study, we also found that Erk phosphorylation level was significantly decreased in SIA-IgG-knockdown LoVo cells (Fig. 5C). To further confirm the role of integrin β4 in the cascade, we suppressed the expression of integrin β4 with specific siRNAs and validated that integrin β4 knockdown indeed decreased the phosphorylation levels of FAK, Src and Erk and the protein levels of p300 and c-Myc in LoVo cells (Supplementary Fig. 6A). Our results suggest that SIA-IgG interacts with integrin β4 and causes activation of the FAK-Src-Erk cascade. Next, we explored whether the effect of exogenous SIA-IgG depends on its Asn162 sialylation. Neuraminidase was used to remove the terminal sialic acids from purified SIA-IgG, and the product was named Neu-IgG (Fig. 5D). SIA-IgG or Neu-IgG was added to SIA-IgG-silencing LoVo cells. We observed that exogenous SIA-IgG, but not Neu-IgG, rescued the phenotypes of SIA-IgG-silencing, including Erk phosphorylation and the protein levels of p300 and c-Myc (Fig. 5E). The result suggests that the sialylation modification of SIA-IgG is essential for the function of SIA-IgG. To investigate the role of activated Erk in SIA-IgG-promoted p300 and c-Myc, we first examined whether Erk activation had an effect on p300 and c-Myc in LoVo cells incubated with Erk1/2 phosphorylation inhibitor U0126 or DMSO for 12 h, and we found that blocking Erk activation with U0126 clearly suppressed p300 and c-Myc protein levels (Fig. 5F). We next examined whether Erk activation was involved in SIA-IgG-induced expression of both p300 and c-Myc. We treated LoVo cells with SIA-IgG purified by RP215-affinity chromatography, non-SIA-IgG (the control-IgG) or PBS in the presence or absence of U0126, and observed the effect of Erk inactivation on p300 and c-Myc protein levels. Our results showed that SIA-IgG increased Erk activation, p300 and c-Myc protein levels, whereas U0126 decreased both basal and SIA-IgG-induced p300 and c-Myc protein levels (Fig. 5G), supporting that Erk1/2 activation indeed mediates the effect of SIA-IgG on p300 and c-Myc.

Taken together, we propose a model whereby SIA-IgG promotes p300 partly dependent on integrin β4-FAK-Src-Erk, leading to the decrease of c-Myc ubiquitination, stabilizing c-Myc protein, guiding CRC cells to develop liver metastasis.

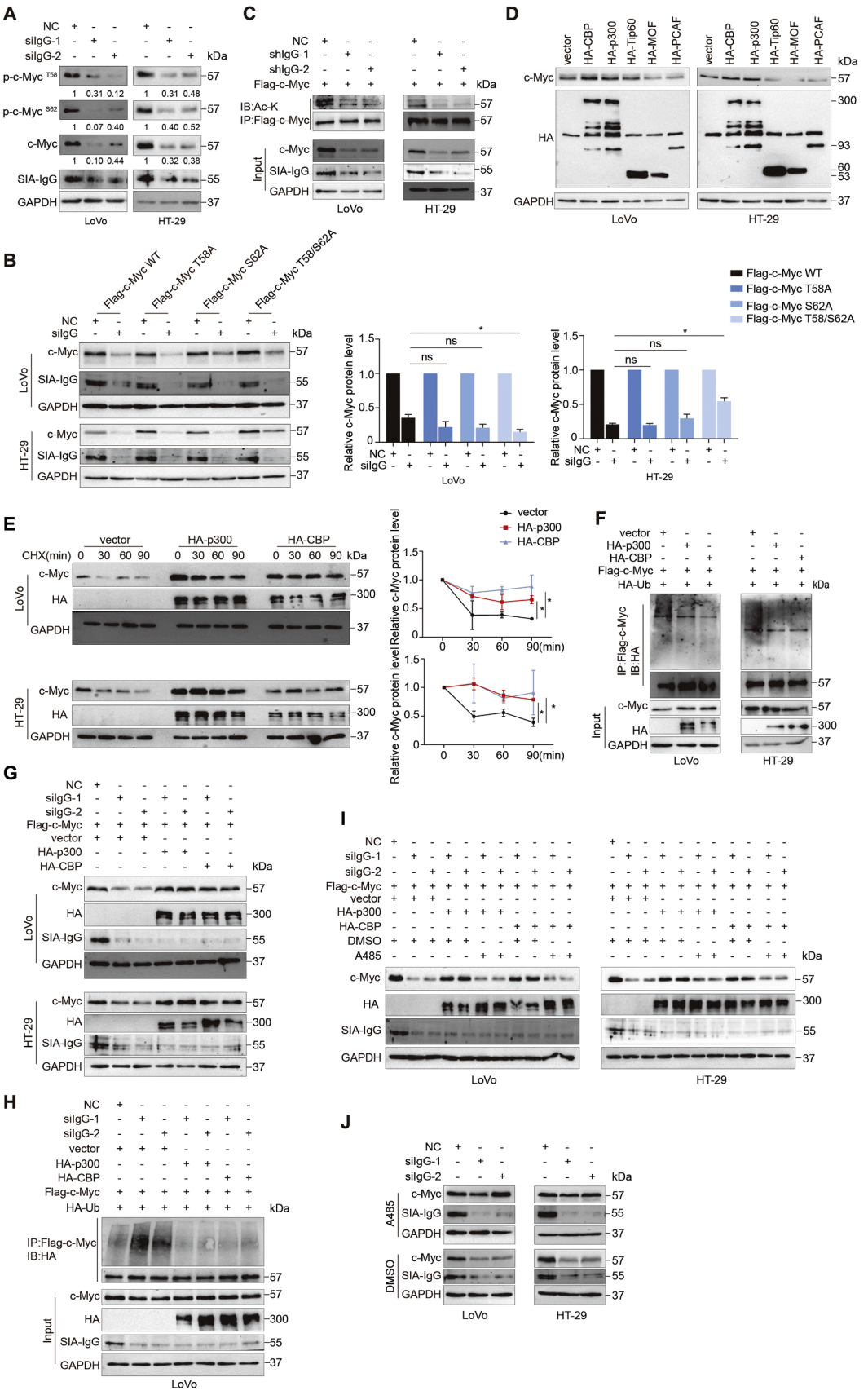

(caption on next page)

Fig. 4. SIA-IgG promotes c-Myc protein stability relying on p300/CBP KAT activities. (A) Western blot analysis showing the total protein and phosphorylation levels of c-Myc in LoVo and HT-29 with SIA-IgG-knockdown or negative control cells. (B) Flag-c-MycWT, Flag-c-MycT58A, Flag-c-MycS62A, Flag-c-MycT58/S62A plasmids were transfected in SIA-IgG knockout LoVo and HT-29 cells. c-Myc protein levels were analyzed via western blotting. (C) The cell lysates of SIA-IgG knockdown LoVo and HT-29 cells treated with trichostatin A (10 μM) and nicotinamide (5 mM) were immunoprecipitated with anti-Flag magnetic beads. And Flag-c-Myc acetylation level was detected. (D) LoVo and HT-29 cells were transfected with vector, HA-CBP, HA-p300, HA-Tip60, HA-MOF and HA-PCAF expression plasmids, c-Myc protein level was analyzed via western blotting. (E) The half-life of the c-Myc protein was analyzed in transiently transfected LoVo and HT-29 cells treated with CHX (200 μg/mL). (F) Immunoprecipitation of Flag-c-Myc using anti-Flag magnetic beads in LoVo and HT-29 cells transfected with the indicated plasmids and treated with MG132 for 10 h. Immunoblot analysis of c-Myc ubiquitination was shown. (G) Negative control and SIA-IgG-knockdown LoVo and HT-29 cells were transfected with vector, HA-p300 or HA-CBP expression plasmids, c-Myc protein level was analyzed via western blotting. (H) Cell lysates of LoVo cells transfected with plasmids as indicated and treated with MG132 (10 μM) for 10 h were subjected to immunoprecipitation. The ubiquitination level of c-Myc was analyzed via immunoblot. (I) LoVo and HT-29 cells were transfected as indicated and treated with DMSO or A485 (3 μM) for 16 h. Western blot was performed as indicated. (J) Cell lysates extracted from the negative control or SIA-IgG knockdown LoVo and HT-29 cell treated with A485 (3 μM) or DMSO for 16 h were subjected to western blot using anti-SIA-IgG and anti-c-Myc antibodies.

Discussion

It is widely accepted that IgG is glycoprotein produced by plasma cells. However, IgG is also observed in various non-B cells [26–29,52] and cancer cells [53]. Notably, IgG produced by epithelial tumors represents unique N-glycosylation at the Asn162 site, which is exactly the epitope recognized by RP215 antibody. Our previous studies have verified that the unique glycosylation modification at Asn162 site of SIA-IgG is critical for its abilities of increasing phosphorylation of c-Met, activation of integrin β4-FAK-Src pathway and interaction with Siglecs, and its functions, including stemness maintenance, cancer cell migration and immune evasion [31,32,37]. In this study, we identify that SIA-IgG is upregulated in CRC. Our previous study reported that SOX2 and OCT4 activate SIA-IgG gene transcription in lung cancer cells [31]. Also, whether sialyltransferases responsible for the addition of a sialic acid participate in the sialylation of SIA-IgG to upregulate SIA-IgG protein expression needs to be explored. Furthermore, we find that SIA-IgG promotes CRC cells proliferation, migration, invasion and liver metastasis in vitro and in vivo. And our findings support the rationale for targeting SIA-IgG with anti-SIA-IgG antibody for CRLM treatment.

It has been reported that the c-Myc is necessary or sufficient for CRC invasion and metastasis by inducing EMT, improving de novo protein biosynthesis or enhancing aerobic glycolysis [54–58]. Moreover, a variety of signaling pathways, including Wnt signaling, mTOR signaling, eukaryotic initiation or elongation factor, microRNAs and lncRNAs, are involved in the regulation of c-Myc in CRC [59]. In this study, our data uncover that the MYC_TARGETS_V1 and MYC_TARGETS_V2 gene sets represent the most significantly downregulated signatures in IgG^{low} patient samples. SIA-IgG dependent on its sialylation modification at Asn162 site upregulates c-Myc protein level by decreasing c-Myc ubiquitination.

Since c-Myc is activated in the vast majority of cancers, it is vital for c-Myc to be tightly regulated. c-Myc can be regulated at levels of DNA amplification [60–62], RNA transcription, stability and translation [63,64] and posttranslational modifications [65]. Phosphorylation, ubiquitination, acetylation and sumoylation are particularly critical for c-Myc expression and protein function. Previous studies show that c-Myc protein can be rapidly stabilized through T58/S62 phosphorylation, which prevents the targeted degradation of c-Myc by the UPS [19]. However, our results show that the T58/S62 phospho-deficient and phosphomimetic c-Myc mutants cannot rescue c-Myc degradation from SIA-IgG knockdown, suggesting that c-Myc is regulated through other ways. Previous reports indicate that c-Myc is acetylated and stabilized by interacting with several KATs, including p300/CBP [14,15], Tip60 [44] and mammalian GCN5 [16]. Our results confirm that p300/CBP extend c-Myc half-life through decreasing c-Myc ubiquitination. Furthermore, p300/CBP can protect c-Myc protein degradation from depletion of SIA-IgG, which is attributed to their acetyltransferase activities. Acetylation of c-Myc inhibits its ubiquitination, resulting in increased c-Myc protein stability. The interplay between acetylation and ubiquitination of c-Myc is not well understood. Since both ubiquitination and acetylation can occur on same lysine residue, two modifications can potentially antagonize with each other. Acetylation decreases ubiquitination of c-Myc and enhances c-Myc stability [15,16] or oncogenic potential [66]. Alternatively, acetylation on c-Myc might affect its affinity binding to E3 ubiquitin ligases or deubiquitinases [67]. In our study, we find that p300/CBP are critical to supporting SIA-IgG-dependent c-Myc protein stability. However, future work is needed to address how p300/CBP acetylating c-Myc impacts on c-Myc ubiquitination.

Previous results support that p300/CBP are essential for the development of CRLM [21,68–70]. Multiple signaling pathways have been identified in the regulation of p300 protein turnover. Phosphorylation of p300 modulated by Erk [48,49], AKT [21,71] and mTOR [72] activation has been shown to promote p300 protein and its acetyltransferase activity. In addition, the degradation of p300/CBP dependent on chaperone-mediated autophagy is mediated by hsc70 and LAMP2A in CRC [73]. Our results suggest that SIA-IgG upregulates p300 protein level through Erk activation in CRLM. Future studies are needed to precisely elucidate how this program works. In our previous study, we find that SIA-IgG specifically interacts with the integrin β4 and activates FAK-Src signaling [32]. We further confirm the role of integrin β4 in the cascade and find that integrin β4 significantly downregulates the phosphorylation levels of FAK, Src and Erk, as well as the protein levels of p300 and c-Myc. The previous study show that Asn162 N-sialylation is vital for the function of SIA-IgG in FAK-Src signaling [32] and Erk activation [31]. Our result show that exogenous SIA-IgG, but not Neu-IgG, rescues the phenotypes of SIA-IgG-silencing, including the phosphorylation of FAK-Src-Erk, the protein levels of p300 and c-Myc, suggesting that the sialylation of SIA-IgG is essential for its function.

In this study, we identify that high IgG expression in CRC is positively correlated with short overall survival and liver metastasis in CRC patients. Moreover, we find that SIA-IgG is overexpressed in CRC and promotes cancer cells migration, invasion and liver metastasis dependent on its unconventional sialylation modification at Asn162 site and that blocking SIA-IgG by RP215 antibody inhibits CRC cells metastasizing to liver in mouse models. Mechanistically, SIA-IgG protects c-Myc from ubiquitin-proteasomal degradation through promoting p300/CBP protein levels. Moreover, p300/CBP stabilize c-Myc via their acetyltransferase activities. Furthermore, SIA-IgG upregulates p300 and c-Myc by activating integrin β4-FAK-Src-Erk signaling. Hence, our results provide novel insights into SIA-IgG promoting CRLM, and offer SIA-IgG as a potential therapeutic strategy for CRLM treatment.

Ethics approval and consent to participate

Colon cancer tissue and distal tissue were obtained from Peking University Peoples' Hospital. And collection of these samples was approved by the Clinical Research Ethics Committee of Peking University Peoples' Hospital (permit number: 2015PHB212-01). Also, informed consents were obtained from participating patients. All animal experiments were approved by Institutional Animal Care and Use Committee of Peking university (permit number: PUIRB-LA2022691).

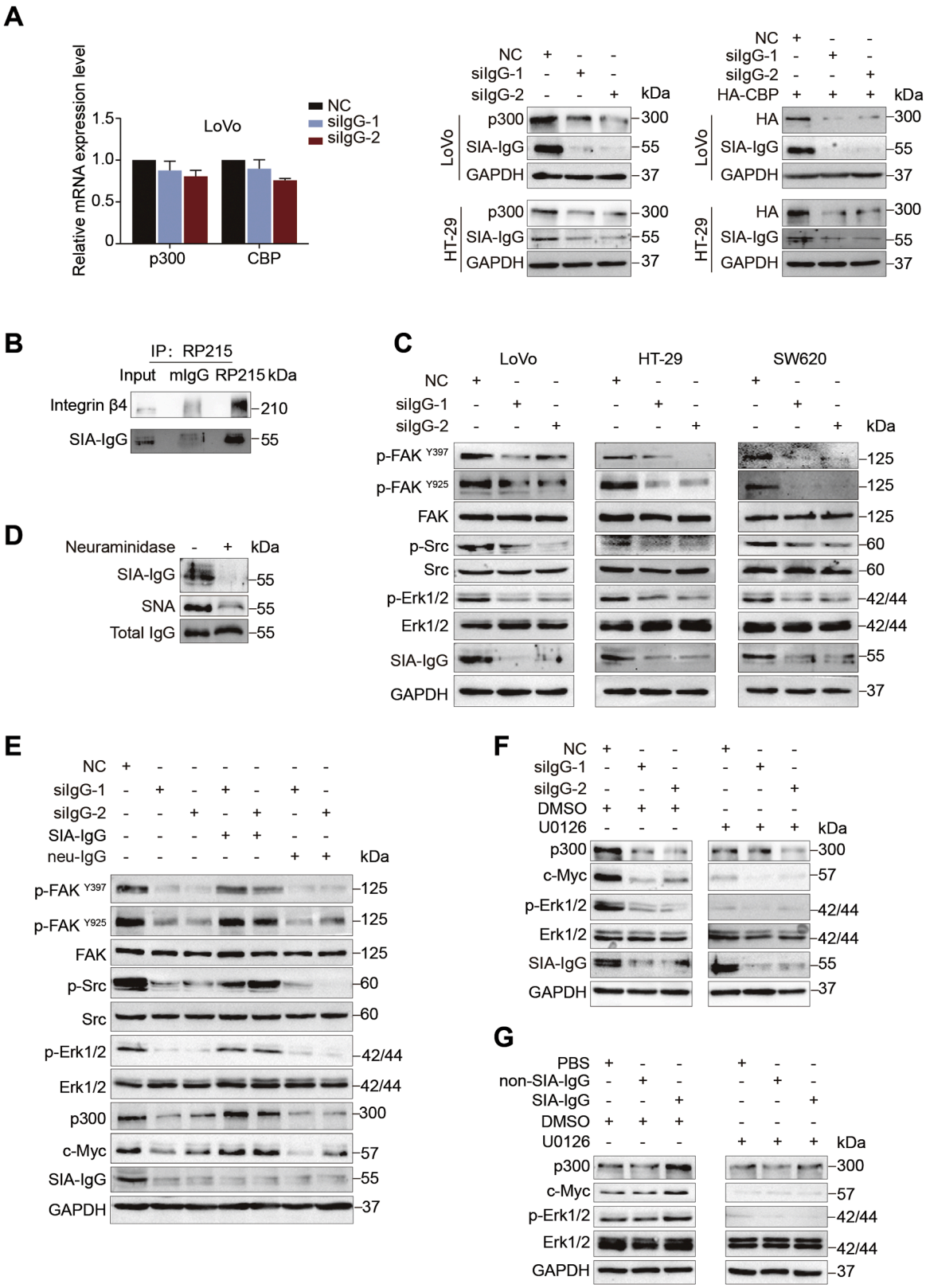

Fig. 5. SIA-IgG modulates p300 and c-Myc through integrin β4-FAK-Src-Erk signaling. (A) LoVo and HT-29 cells were transfected as indicated. The mRNA expression levels of p300 and CBP were assessed by RT-PCR (left panel) and western blot (right panel) was performed to determine p300 and HA-CBP protein levels. (B) Co-IP assay was performed to detect the interaction between SIA-IgG and integrin β4 in LoVo cells. (C) The phosphorylation levels of FAK, Src and Erk were detected via western blotting in SIA-IgG silencing or negative control LoVo, HT-29 and SW620 cells. (D) Purified SIA-IgG protein was digested by neuraminidase, and SIA-IgG, SNA lectin and IgG were detected by western blot. (E) SIA-IgG-knockdown cells were treated with purified SIA-IgG or SIA-IgG digested by neuraminidase and the indicated proteins were analyzed by western blot. (F) LoVo cells were transiently transfected with siRNA targeting IgG or non-targeting control siRNA, and incubated in the presence or absence of U0126 (10 μM) for 12 h. Whole cell lysates were prepared, and western blot was performed. (G) LoVo cells were treated with SIA-IgG, non-SIA-IgG or PBS for 24 h, and incubated in the presence or absence of U0126 (10 μM) for 12 h, and cell lysates were harvested and detected by western blotting.

CRediT authorship contribution statement

Jing Chen: Conceptualization, Data curation, Formal analysis, Investigation, Methodology, Software, Validation, Visualization, Writing – original draft. **Shenghua Zhang:** Data curation, Formal analysis, Methodology, Software, Resources. **Xinmei Huang:** Conceptualization, Formal analysis, Methodology. **Qianqian Wang:** Methodology, Investigation, Data curation. **Weiyan Xu:** Methodology, Resources. **Jing Huang:** Conceptualization, Methodology, Resources, Supervision. **Yuming Su:** Methodology. **Qinkun Sun:** Methodology. **Xiaojuan Du:** Conceptualization, Resources, Visualization, Writing – review & editing. **Baocai Xing:** Conceptualization, Methodology, Resources, Supervision. **Xiaoyan Qiu:** Conceptualization, Funding acquisition, Resources, Supervision, Visualization, Writing – review & editing.

Declaration of competing interest

The authors declare that they have no known competing financial interests or personal relationships that could have appeared to influence the work reported in this paper.

Acknowledgements

We would like to thank Lina Wu (Peking University) for providing SW620 cell line, Yingyu Chen (Peking University) for donating c-Myc plasmid, and Jianyuan Luo (Peking University) for gifting HA-p300, HA-CBP, HA-Tip60, HA-PCAF and HA-MOF plasmids. This study was supported by research grants to Xiaoyan Qiu from Key Projects of the National Natural Science Foundation of China (No.82030044 and 82341227).

Supplementary materials

Supplementary material associated with this article can be found, in the online version, at doi:10.1016/j.neo.2025.101140.

References

[1] H. Sung, J. Ferlay, R.L. Siegel, M. Laversanne, I. Soerjomataram, A. Jemal, et al., Global Cancer statistics 2020: GLOBOCAN estimates of incidence and mortality worldwide for 36 cancers in 185 countries, CA: Cancer J. Clin. 71 (2021) 209–249.
[2] D.I. Tsilimigras, P. Brodt, P.-A. Clavien, R.J. Muschel, M.I. D'Angelica, I. Endo, et al., Liver metastases, Nat. Rev. Dis. Prim. 7 (2021) 27.
[3] D. Hanahan, Hallmarks of cancer: new dimensions, Cancer Discov. 12 (2022) 31–46.
[4] A. Wolfer, S. Ramaswamy, MYC and metastasis, Cancer Res. 71 (2011) 2034–2037.
[5] H. Li, N. Zheng, A. Guo, W. Tang, M. Li, Y. Cao, et al., FSTL3 promotes tumor immune evasion and attenuates response to anti-PD1 therapy by stabilizing c-Myc in colorectal cancer, Cell Death Dis. 15 (2024) 107.
[6] Z. Lv, J. Wei, W. You, R. Wang, J. Shang, Y. Xiong, et al., Disruption of the c-Myc/miR-200b-3p/PRDX2 regulatory loop enhances tumor metastasis and chemotherapeutic resistance in colorectal cancer, J. Transl. Med. 15 (2017) 257.
[7] S. Nicklas, A.-L. Hillje, S. Okawa, I.-M. Rudolph, F.M. Collmann, T. van Wuellen, et al., A complex of the ubiquitin ligase TRIM32 and the deubiquitinase USP7 balances the level of c-myc ubiquitination and thereby determines neural stem cell fate specification, Cell Death Differen. 26 (2019) 728–740.
[8] K. Li, F. Wang, Z.N. Yang, T.T. Zhang, Y.F. Yuan, C.X. Zhao, et al., TRIB3 promotes MYC-associated lymphoma development through suppression of UBE3B-mediated MYC degradation, Nat. Commun. 11 (2020) 6316.
[9] X. Han, C. Ren, C. Lu, P. Qiao, T. Yang, Z. Yu, Deubiquitination of MYC by OTUB1 contributes to HK2 mediated glycolysis and breast tumorigenesis, Cell Death Differen. 29 (2022) 1864–1873.
[10] J. Pan, Q. Deng, C. Jiang, X. Wang, T. Niu, H. Li, et al., USP37 directly deubiquitinates and stabilizes c-myc in lung cancer, Oncogene 34 (2015) 3957–3967.
[11] J. Wang, Y. Yang, F. Shao, Y. Meng, D. Guo, J. He, et al., Acetate reprogrammes tumour metabolism and promotes PD-L1 expression and immune evasion by upregulating c-Myc, Nat. Metabol. 6 (2024) 914–932.
[12] A.L. Huber, S.J. Papp, A.B. Chan, E. Henriksson, S.D. Jordan, A. Kriebs, et al., CRY2 and FBXL3 cooperatively degrade c-MYC, Mol. Cell 64 (2016) 774–789.
[13] A.V. Vaseva, D.R. Blake, T.S.K. Gilbert, S. Ng, G. Hostetter, S.H. Azam, et al., KRAS suppression-induced degradation of MYC is antagonized by a MEK5-ERK5 compensatory mechanism, Cancer Cell 34 (2018) 807–822, e7.
[14] D. Jiao, R. Sun, X. Ren, Y. Wang, P. Tian, Y. Wang, et al., Lipid accumulation-mediated histone hypoacetylation drives persistent NK cell dysfunction in anti-tumor immunity, Cell Rep. 43 (2024) 113632.
[15] J. Vervoorts, J.M. Lüscher-Firzlaff, S. Rottmann, R. Lilischkis, G. Walsemann, K. Dohmann, et al., Stimulation of c-MYC transcriptional activity and acetylation by recruitment of the cofactor CBP, EMBO Rep. 4 (2003) 484–490.
[16] J.H. Patel, Y. Du, P.G. Ard, C. Phillips, B. Carella, C.J. Chen, et al., The c-MYC oncoprotein is a substrate of the acetyltransferases hGCN5/PCAF and TIP60, Mol. Cell Biol 24 (2004) 10826–10834.
[17] L.M. Mustachio, J. Roszik, A.T. Farria, K. Guerra, S.Y. Dent, Repression of GCN5 expression or activity attenuates c-MYC expression in non-small cell lung cancer, Am. J. Cancer Res. 9 (2019) 1830–1845.
[18] J.M. Lee, H.M. Hammarén, M.M. Savitski, S.H. Baek, Control of protein stability by post-translational modifications, Nat. Commun. 14 (2023) 201.
[19] A.S. Farrell, R.C. Sears, MYC degradation, Cold Spring Harb. Perspect. Med. 4 (2014).
[20] C.V. Dang, E.P. Reddy, K.M. Shokat, L. Soucek, Drugging the 'undruggable' cancer targets, Nat. Rev. Cancer 17 (2017) 502–508.
[21] C. Dou, Z. Liu, K. Tu, H. Zhang, C. Chen, U. Yaqoob, et al., P300 Acetyltransferase mediates stiffness-induced activation of hepatic stellate cells into tumor-promoting myofibroblasts, Gastroenterology 154 (2018) 2209–2221, e14.
[22] Y. Liu, E.J. Yang, C. Shi, P.K. Mou, B. Zhang, C. Wu, et al., Histone acetyltransferase (HAT) P300/CBP inhibitors induce synthetic lethality in PTEN-deficient colorectal cancer cells through destabilizing AKT, Int. J. Biol. Sci. 16 (2020) 1774–1784.
[23] J. Liu, P300 increases CSNK2A1 expression which accelerates colorectal cancer progression through activation of the PI3K-AKT-mTOR axis, Exp. Cell Res. 430 (2023) 113694.
[24] S. Jain, J. Wei, L.R. Mitrani, N.H. Bishopric, Auto-acetylation stabilizes p300 in cardiac myocytes during acute oxidative stress, promoting STAT3 accumulation and cell survival, Breast Cancer Res. Treat 135 (2012) 103–114.
[25] T. Du, Y. Nagai, Y. Xiao, M.I. Greene, H. Zhang, Lysosome-dependent p300/FOXP3 degradation and limits treg cell functions and enhances targeted therapy against cancers, Exp. Mol. Pathol. 95 (2013) 38–45.
[26] N. Niu, J. Zhang, Y. Guo, Y. Zhao, C. Korteweg, J. Gu, Expression and distribution of immunoglobulin G and its receptors in the human nervous system, Int. J. Biochem. Cell Biol. 43 (2011) 556–563.
[27] Y. Lei, T. Huang, M. Su, J. Luo, C. Korteweg, J. Li, et al., Expression and distribution of immunoglobulin G in the normal liver, hepatocarcinoma and postpartial hepatectomy liver, Lab. Invest. 94 (2014) 1283–1295.
[28] M. Yan, X. Zhang, Q. Pu, T. Huang, Q. Xie, Y. Wang, et al., Immunoglobulin G expression in human sperm and possible functional significance, Sci. Rep. 6 (2016) 20166.
[29] Z. zhu, M. Zhang, W. Shao, P. Wang, X. Gong, J. Ma, et al., Immunoglobulin M, a novel molecule of myocardial cells of mice, Int. J. Biochem. Cell Biol. 88 (2017) 172–180.
[30] C. Ma, Y. Wang, G. Zhang, Z. Chen, Y. Qiu, J. Li, et al., Immunoglobulin G expression and its potential role in primary and metastatic breast cancers, Curr. Mol. Med. 13 (2013) 429–437.
[31] X. Huang, S. Zhang, J. Tang, T. Tian, Y. Pan, L. Wu, et al., A self-propagating c-met–SOX2 axis drives cancer-derived IgG signaling that promotes lung cancer cell stemness, Cancer Res. 83 (2023) 1866–1882.
[32] J. Tang, J. Zhang, Y. Liu, Q. Liao, J. Huang, Z. Geng, et al., Lung squamous cell carcinoma cells express non-canonically glycosylated IgG that activates integrin-FAK signaling, Cancer Lett. 430 (2018) 148–159.
[33] C. Qin, Z. Sheng, X. Huang, J. Tang, Y. Liu, T. Xu, et al., Cancer-driven IgG promotes the development of prostate cancer though the SOX2-CIgG pathway, Prostate 80 (2020) 1134–1144.
[34] M. Cui, L. You, B. Zheng, X. Huang, Q. Liu, J. Huang, et al., Erratum: high expression of cancer-derived glycosylated immunoglobulin G predicts poor prognosis in pancreatic ductal adenocarcinoma: erratum, J Cancer 12 (2021) 6497.
[35] Z. Chen, J. Gu, Immunoglobulin G expression in carcinomas and cancer cell lines, Faseb J. 21 (2007) 2931–2938.
[36] Y. Mimura, T. Katoh, R. Saldova, R. O'Flaherty, T. Izumi, Y. Mimura-Kimura, et al., Glycosylation engineering of therapeutic IgG antibodies: challenges for the safety, functionality and efficacy, Protein Cell 9 (2017) 47–62.
[37] Z. Wang, Z. Geng, W. Shao, E. Liu, J. Zhang, J. Tang, et al., Cancer-derived sialylated IgG promotes tumor immune escape by binding to Siglecs on effector T cells, Cell. Mol. Immunol. 17 (2020) 1148–1162.
[38] H. Jiang, B. Kang, X. Huang, Y. Yan, S. Wang, Y. Ye, et al., Cancer IgG, a potential prognostic marker, promotes colorectal cancer progression, Chin. J. Cancer Res. 31 (2019) 499–510.
[39] C. Li, Z. Tang, W. Zhang, Z. Ye, F. Liu, GEPIA2021: integrating multiple deconvolution-based analysis into GEPIA, Nucl. Acids Res. 49 (2021) W242–W2W6.
[40] C. Li, Y.D. Sun, G.Y. Yu, J.R. Cui, Z. Lou, H. Zhang, et al., Integrated omics of metastatic colorectal cancer, Cancer Cell 38 (2020) 734–747, e9.
[41] V. Mittal, Epithelial mesenchymal transition in tumor metastasis, Annu. Rev. Pathol. 13 (2018) 395–412.
[42] A.E. Shin, F.G. Giancotti, A.K. Rustgi, Metastatic colorectal cancer: mechanisms and emerging therapeutics, Trends Pharmacol. Sci. 44 (2023) 222–236.
[43] N. Zhang, A.S. Ng, S. Cai, Q. Li, L. Yang, D. Kerr, Novel therapeutic strategies: targeting epithelial–mesenchymal transition in colorectal cancer, Lancet Oncol. 22 (2021) e358–ee68.

[44] X. Wei, S. Cai, R.J. Boohaker, J. Fried, Y. Li, L. Hu, et al., KAT5 promotes invasion and metastasis through C-MYC stabilization in ATC, Endocr. Relat. Cancer 26 (2019) 141–151.
[45] W. Xu, L. Xie, Y. Yang, J. Xu, S. Cai, Y. Tian, KAT5 Inhibitor NU9056 suppresses anaplastic thyroid carcinoma progression through c-myc/miR-202 pathway, Int. J. Endocrinol. 2022 (2022) 2014568.
[46] K. Zhang, F. Faiola, E. Martinez, Six lysine residues on c-Myc are direct substrates for acetylation by p300, Biochem. Biophys. Res. Commun. 336 (2005) 274–280.
[47] L.M. Lasko, C.G. Jakob, R.P. Edalji, W. Qiu, D. Montgomery, E.L. Digiammarino, et al., Discovery of a selective catalytic p300/CBP inhibitor that targets lineage-specific tumours, Nature 550 (2017) 128–132.
[48] J.H. Jun, W.J. Yoon, S.B. Seo, et al., BMP2-activated Erk/MAP kinase stabilizes Runx2 by increasing p300 levels and histone acetyltransferase activity, J. Biol. Chem. 285 (47) (2010) 36410–36419, https://doi.org/10.1074/jbc.M110.142307.
[49] Y.J. Chen, Y.N. Wang, W.C. Chang, ERK2-mediated C-terminal serine phosphorylation of p300 is vital to the regulation of epidermal growth factor-induced keratin 16 gene expression, J. Biol. Chem. 282 (37) (2007) 27215–27228, https://doi.org/10.1074/jbc.M700264200.
[50] Y.H. Huang, H.K. Chen, Y.F. Hsu, H.C. Chen, C.H. Chuang, S.W. Huang, et al., Src-FAK signaling mediates interleukin 6-induced HCT116 colorectal cancer epithelial-mesenchymal transition, Int. J. Mol. Sci. 24 (2023).
[51] X. Chen, J. Chen, W. Feng, W. Huang, G. Wang, M. Sun, et al., FGF19-mediated ELF4 overexpression promotes colorectal cancer metastasis through transactivating FGFR4 and SRC, Theranostics 13 (2023) 1401–1418.
[52] N. Niu, J. Zhang, Y. Sun, S. Wang, Y. Sun, C. Korteweg, et al., Expression and distribution of immunoglobulin G and its receptors in an immune privileged site: the eye, Cell Mol. Life Sci. 68 (2011) 2481–2492.
[53] M. Cui, J. Huang, S. Zhang, Q. Liu, Q. Liao, X. Qiu, Immunoglobulin expression in cancer cells and its critical roles in tumorigenesis, Front. Immunol. 12 (2021) 613530.
[54] Z. Wei, C. Mu-Yan, T. Zhu-Ting, D. Sui-Sui, M. Shi-Juan, L. Yi-Ji, et al., Overexpression of EIF5A2 promotes colorectal carcinoma cell aggressiveness by upregulating MTA1 through C-myc to induce epithelial–mesenchymaltransition, Gut 61 (2012) 562.
[55] Q. Tang, J. Chen, Z. Di, W. Yuan, Z. Zhou, Z. Liu, et al., TM4SF1 promotes EMT and cancer stemness via the wnt/β-catenin/SOX2 pathway in colorectal cancer, J. Exp. Clin. Cancer Res. 39 (2020) 232.
[56] C. Liu, M. Rokavec, Z. Huang, H. Hermeking, Salicylate induces AMPK and inhibits c-MYC to activate a NRF2/ARE/miR-34a/b/c cascade resulting in suppression of colorectal cancer metastasis, Cell Death Dis. 14 (2023) 707.
[57] L.P. Loevenich, M. Tschurtschenthaler, M. Rokavec, M.G. Silva, M. Jesinghaus, T. Kirchner, et al., SMAD4 Loss induces c-MYC–Mediated NLE1 upregulation to support protein biosynthesis, colorectal cancer growth, and metastasis, Cancer Res. 82 (2022) 4604–4623.
[58] J. Wu, Q. Chen, Y. Wang, R. Wang, Q. Chen, Y. Wang, et al., LINC01977 promotes colorectal cancer growth and metastasis by enhancing aerobic glycolysis via the ERK/c-Myc axis, J. Gastrointest. Oncol. 15 (2024) 271–285.
[59] L. Tan, D. Peng, Y. Cheng, Significant position of C-myc in colorectal cancer: a promising therapeutic target, Clin. Transl. Oncol. 24 (2022) 2295–2304.
[60] L.S. Pongor, C.W. Schultz, L. Rinaldi, D. Wangsa, C.E. Redon, N. Takahashi, et al., Extrachromosomal DNA amplification contributes to small cell lung cancer heterogeneity and is associated with worse outcomes, Cancer Discov. 13 (2023) 928–949.
[61] R. Maddipati, R.J. Norgard, T. Baslan, K.S. Rathi, A. Zhang, A. Saeid, et al., MYC levels regulate metastatic heterogeneity in pancreatic adenocarcinoma, Cancer Discov. 12 (2022) 542–561.
[62] D.J.H. Shih, N. Nayyar, I. Bihun, I. Dagogo-Jack, C.M. Gill, E. Aquilanti, et al., Genomic characterization of human brain metastases identifies drivers of metastatic lung adenocarcinoma, Nat. Genet. 52 (2020) 371–377.
[63] H. Huang, H. Weng, W. Sun, X. Qin, H. Shi, H. Wu, et al., Recognition of RNA N6-methyladenosine by IGF2BP proteins enhances mRNA stability and translation, Nat. Cell Biol. 20 (2018) 285–295.
[64] R. Tu, Z. Chen, Q. Bao, H. Liu, G Qing, Crosstalk between oncogenic MYC and noncoding RNAs in cancer, Sem. Cancer Biol. 75 (2021) 62–71.
[65] J. Vervoorts, J. Lüscher-Firzlaff, B. Lüscher, The ins and outs of MYC regulation by posttranslational mechanisms, J. Biol. Chem. 281 (2006) 34725–34729.
[66] T. Muto, M. Guillamot, J. Yeung, J. Fang, J. Bennett, B. Nadorp, et al., TRAF6 functions as a tumor suppressor in myeloid malignancies by directly targeting MYC oncogenic activity, Cell Stem Cell 29 (2022) 298–314, e9.
[67] H. Wu, T.Y. Yang, Y. Li, W.L. Ye, F. Liu, X.S. He, et al., Tumor necrosis factor receptor-associated factor 6 promotes hepatocarcinogenesis by interacting with histone deacetylase 3 to enhance c-myc gene expression and protein stability, Hepatology 71 (2020) 148–163.
[68] Z. Wu, D. Wei, W. Gao, Y. Xu, Z. Hu, Z. Ma, et al., TPO-induced metabolic reprogramming drives liver metastasis of colorectal cancer CD110+ tumor-initiating cells, Cell Stem Cell 17 (2015) 47–59.
[69] W. Lu, C. Yang, H. He, H. Liu, The CARM1-p300-c-Myc-Max (CPCM) transcriptional complex regulates the expression of CUL4A/4B and affects the stability of CRL4 E3 ligases in colorectal cancer, Int. J. Biol. Sci. 16 (2020) 1071–1085.
[70] C. Liu, Q. Yang, Q. Zhu, X. Lu, M. Li, T. Hou, et al., CBP mediated DOT1L acetylation confers DOT1L stability and promotes cancer metastasis, Theranostics 10 (2020) 1758–1776.
[71] W.C. Huang, C.C. Chen, Akt phosphorylation of p300 at ser-1834 is essential for its histone acetyltransferase and transcriptional activity, Mol. Cell Biol. 25 (2005) 6592–6602.
[72] W. Wan, Z. You, Y. Xu, L. Zhou, Z. Guan, C. Peng, et al., mTORC1 Phosphorylates acetyltransferase p300 to regulate autophagy and lipogenesis, Mol. Cell 68 (2017) 323–335, e6.
[73] C. Du, D. Huang, Y. Peng, Y. Yao, Y. Zhao, Y. Yang, et al., 5-Fluorouracil targets histone acetyltransferases p300/CBP in the treatment of colorectal cancer, Cancer Lett. 400 (2017) 183–193.